Design of PVDF/PEGMA- b -PS- b -PEGMA membranes by VIPS for improved biofouling mitigation

Séverine Carretier, Li-An Chen, Antoine Venault, Zhong-Ru Yang, Pierre Aimar, Yung Chang

Design of PVDF/PEGMA-*b*-PS-*b*-PEGMA membranes by VIPS for improved biofouling mitigation

Séverine Carretier [a], Li-An Chen [a], Antoine Venault [a,*], Zhong-Ru Yang [a], Pierre Aimar [b], Yung Chang [a,*]

[a] *R&D Center for Membrane Technology and Department of Chemical Engineering, Chung Yuan Christian University, Chung-Li 32023, Taiwan*
[b] *Laboratoire de Génie Chimique, Université Paul Sabatier, 118 route de Narbonne, 31062 Toulouse Cedex 9, France*

Keywords:
PVDF membrane
PEGMA-*b*-PS-*b*-PEGMA copolymer
VIPS process
Membrane formation
Low-biofouling

A B S T R A C T

Literature on the design of efficient nonfouling membranes by *in-situ* modification is poor, which can be explained by the difficulty to control membrane formation mechanisms when a third material is added to the casting solution, or by the lack of stability of matrix polymers with surface-modifiers. We present polyvinylidene fluoride membranes formed by vapor-induced phase separation and modified with a tri-block copolymer of poly(styrene) and poly(ethylene glycol) methacrylate moieties ($PEGMA_{124}$-*b*-PS_{54}-*b*-$PEGMA_{124}$). After characterizing the copolymer, we move onto membrane formation mechanisms. Membrane formation is well controlled and leads to structure close to bi-continuous. Considering the formulation chosen, PVDF/$PEGMA_{124}$-*b*-PS_{54}-*b*-$PEGMA_{124}$ solutions are less viscous and more hydrophilic than virgin PVDF solutions. Both effects promote non-solvent transfer, thus decreasing the chances for crystallization. Hydrophilic capability of membranes is increased from about 59 mg/cm^3 to 650 mg/cm^3, leading to a severe drop of non-specific protein adsorption, up to 85–90%, also depending on its nature. Biofouling at the micro-scale by modified *Escherichia coli* and *Streptococcus mutans* is almost totally inhibited. Finally, biofouling is importantly reduced in dynamic conditions, as measured from the water flux recovery ratio of 69.4%, after 3 water-BSA filtration cycles, much higher than with a commercial hydrophilic PVDF membrane (47.3%). These membranes hold promise as novel materials for water-treatment or blood filtration.

1. Introduction

The search for the perfect nonfouling porous membrane remains one of the major targets of membranologists worldwide, as fouling arises from a complex interplay of physical and chemical phenomena that are difficult to anticipate. Another reason explaining this endless search is linked to the well-established structure-property relationships of materials. For instance, reducing the pore size and making a smoother interface shall permit to physically mitigate fouling, but the downside is a logical decrease of membrane permeability.

As resistance to fouling and in particular to biofouling is recognized to be closely linked to the ability of polymer chains to be surrounded by a protective hydration layer [1], it is harder to achieve with hydrophobic polymers, such as poly(vinylidene fluoride), polypropylene or poly(tetrafluoride ethylene). Yet, these polymers are of major interest for their excellent bulk properties. As far as PVDF is concerned, it is relatively inexpensive, chemically and thermally stable, and membranes from PVDF can be readily prepared by wet-immersion process, such that applications of PVDF membranes are countless. Therefore, numerous teams including ours have focused their efforts on the design of nonfouling or at least low fouling PVDF membranes [2–8].

A number of routes exist to prepare nonfouling membranes, going from surface modification processes to direct *in*-situ modification [1,9]. Surface modification processes involve self-assembling methods, for which physical interactions are established between the matrix polymer and the modifier [10,11], and chemical surface modification processes, arising in more stable interactions between the membrane and the nonfouling moieties [12–14]. These two-step processes are probably the most commonly tested by researchers in their quest for nonfouling membranes, as commercial membranes with controlled porous structure are often used as substrates. Nevertheless, these methods have two drawbacks: they are lengthy and they only permit to modify the top-layers of the membrane. By lengthy, it is considered here that membrane must be prepared (or purchased)

* Corresponding authors.
E-mail addresses: avenault@cycu.edu.tw (A. Venault), ychang@cycu.edu.tw (Y. Chang).

before being surface-modified, and at least two unit operations are required. As for the second disadvantage, it would not be a major issue if the top-layer was perfectly nonfouling as biofoulants would be repelled. But nonfouling property does not exist yet for porous membranes, as far as we know. So, foulants managing to permeate through the protective layer can then easily interact with the matrix in the layers underneath, and lead to partial pore blockage. In this respect, *in-situ* modification, in which formation and modification are done all at once [6,15–17], can potentially address these issues. In these methods however, the question of formation mechanisms remain hard to address and structure control is challenging. The effect of surface-modifier (often a block or random copolymer) is often seen and often unpredictable, at a same copolymer can act as a pore-former or as a pore suppressor, depending on its concentration [18]. Therefore, a careful study of the effect of copolymer on membrane formation should be systematically ran in parallel to that on nonfouling properties of membranes.

Lately, there has been significant progress made regarding the stability of matrix modification by *in-situ* modification, using water-insoluble copolymers [19–22], and the examination of fouling resistance at the nano-scale (involving proteins) remains today a major research direction [23,24]. However, we still face numerous challenges. First, it is noticed that researchers using water-insoluble copolymers actually synthesized a copolymer which is a combination of the matrix polymer and hydrophilic blocks [20–22]. This enables facilitating the blending, intermolecular interactions and cross-linking with the original un-modified polymer, but it narrows the possibilities of application of the copolymer with other polymers, that is the preparation of other membranes. The second issue is linked to the structure: except the very few previous studies in which precipitation from the vapor-phase is used [6,25], formation of antifouling membranes is usually done by wet-immersion using water as non-solvent, which eventually leads to finger-like structures [19–22], and presenting a skin layer more or less porous. These membranes are known to be relatively weak and their permeability not always optimal as the polymer-poor domains are not interconnected. A way to address this need is to further develop the formation of antifouling membranes by other routes, such as the vapor-induced phase separation. Thirdly, the antifouling properties of porous (and non-porous) membranes can still be improved, and in particular their resistance to non-specific protein adhesion. In particular, in the case of porous matrix, pores offer a penalty to fouling. It means that physical entrapment of biofoulants occurs more easily. In order to reduce physical trapping, chemical surface and bulk modification should be made more efficient, by developing new antifouling polymers, able to ensure optimal surface modification (measured through the coating density or grafting density when a surface-modification is at play) or bulk modification. Tri-block copolymers possessing two hydrophilic blocks and one anchor hydrophobic block can probably better answer these needs than di-block copolymers having only one single hydrophilic block.

Based on these needs, we have developed an amphiphilic tri-block copolymers, containing two hydrophilic blocks of poly (ethylene glycol) methacrylate and one anchor hydrophobic block of polystyrene. The first part of this work presents the complete characterization of this triblock PEGMA$_{124}$-*b*-PS$_{54}$-*b*-PEGMA$_{124}$ copolymer. Then, we lay the focus on some formation aspects of PVDF/PEGMA$_{124}$-*b*-PS$_{54}$-*b*-PEGMA$_{124}$ membranes by vapor-induced phase separation, and characterize the kinetic and thermodynamic of phase separation, leading to structures close to bi-continuous, as well as we investigate the efficiency of surface modification. In a third part, we focus on anti-fouling properties of these membranes in both static and dynamic conditions. We hope to demonstrate that the VIPS process applied to the PVDF/PEGMA$_{124}$-*b*-PS$_{54}$-*b*-PEGMA$_{124}$/NMP system is an ideal avenue toward the formation of efficient and stiff microfiltration membranes with controlled porous structure.

2. Materials and methods

2.1. Materials

Poly(vinylidene fluoride) (PVDF) polymer was bought from Kynar®. It has a molecular weight (Mw) of about 150,000 g mol^{-1}. It was first washed with methanol and DI water before use in casting solutions in order to remove impurities. The tri-block PEGMA$_{124}$-*b*-PS$_{54}$-*b*-PEGMA$_{124}$ copolymer used in this study was synthesized from styrene monomer (Mw = 104.15 g/mol, Fluka) and poly (ethylene glycol) methacrylate (PEGMA) homopolymer (Mw = 475 g/mol, Aldrich) as detailed in next section. 2-(((1-carboxy-1-methylethylsulfanyl)thiocarbonyl)sulfanyl)-2-methylpropionic (Mw = 282.41 g/mol) was synthesized in the lab. 4,4′-Azobis (4-cyanovaleric acid) (Mw = 280.28 g/mol, Alfa Aesar), toluene (Sigma Aldrich) and hexane (Sigma Aldrich) were also used for the polymerization reaction. Solvent used for membrane preparation was *N*-methylpyrrolidone (NMP), purchased from Tedia, and directly used without purification. Finally, DI water (minimum resistivity of 18.0 MΩ cm), was used as a non-solvent in membrane preparation, and in different characterization steps. It was obtained from a Millipore purification system.

2.2. Methods

2.2.1. Synthesis of tri-block copolymers

The tri-block copolymer was synthesized by reverse radical addition-fragment chain transfer (RAFT) (Fig. S1). First, PEGMA-raft reagent was synthesized. PEGMA, 4,4′-Azobis(4-cyanovaleric acid) (initiator) and 2-(((1-carboxy-1-methylethylsulfanyl)thiocarbonyl)sulfanyl)-2-methylpropionic (reagent) were mixed in toluene. Before reaction, nitrogen was bubbled into the solution for 15 min to purge oxygen. The total solid content was 20 wt%, and the [PEGMA]:[Initiator]:[Reagent] molar ratio was 500:0.2:1. Reaction was performed at 80 °C, for 24 h. Then, the reaction was stopped by immersing the reaction flask into a ice bath, for 30 min. Copolymer was precipitated using hexane as a non-solvent (the volume of hexane added was twenty times that of toluene), and then freeze-dried (EYLA FDU-1200) until reaching constant weight.

The second step consisted in mixing styrene monomer, initiator and PEGMA-RAFT reagent (80:0.2:1) in toluene, fixing the dry weight content to 20 wt%. Similarly, the solution was purged before the reaction. The polymerization was performed at 80 °C, for 24 h. It was then stopped using an ice bath, and the tri-block copolymer obtained was precipitated with hexane (the volume of hexane added was twenty times that of toluene), and then freeze-dried (EYLA FDU-1200) until reaching constant weight.

2.2.2. Characterization of tri-block copolymers

The chemical structure of *tri-block* copolymer was assessed by ^{1}H NMR spectrometry using a 500 MHz spectrometer (Bruker) and chloroform-d as solvent. Concentration of copolymer in solvent was 5 mg/mL. Gas phase chromatography (GPC) analysis was also performed with a THF gel permeation chromatograph (ViscotekGPCmax Module, USA). For this analysis, a Jordi Gel CN15073 column (Mw range 100–20 kDa) was connected to a VE3580 refractive index detector. Flow rate was set to 1.0 mL/min flow and column temperature maintained to 25 °C. PS standards (American Polymer Standards Corp., USA) were used for calibration.

Table 1
Composition of casting solutions leading to virgin and PEGylated PVDF membranes.

Membrane ID	PVDF (wt%)	$PEGMA_{124}$-*b*-PS_{54}-*b*-$PEGMA_{124}$ (wt%)	NMP (wt%)	Viscosity (Pa.s)
P25-TB0	25	0	75	5.276 ± 0.051
P24-TB1	24	1	75	/
P23-TB2	23	2	75	/
P22-TB3	22	3	75	/
P21-TB4	21	4	75	/
P20-TB5	20	5	75	3.261 ± 0.006

2.2.3. Preparation of casting solutions

Solutions were prepared by blending PVDF and $PEGMA_{124}$-*b*-PS_{54}-*b*-$PEGMA_{124}$ in NMP. 6 solutions were prepared, one containing PVDF only and 5 containing both PVDF and triblock copolymer. The concentration of PVDF was decreased from 25 wt% to 20 wt%, while that of copolymer increased from 0 to 5 wt%. Therefore concentration of NMP was the same in all casting solutions (Table 1). Solutions were stirred at relatively low temperature, 35 °C, to reduce the chances for membrane formation by crystallization during subsequent membrane preparation step [26,27]. This point will be further discussed later in this manuscript. Dissolution time took about 3 days. Once apparently homogeneous, solutions were allowed to rest for a few hours until they stopped bubbling, and immediately cast.

Viscosity of some casting solutions was determined at 25 °C with a BROOKFIELD R/S Rheometer and at constant share rate ($100\ s^{-1}$). Temperature was regulated by a FIRSTEK water-bath. The module employed was a C50-1 (disk shape).

2.2.4. Preparation of membranes

Membranes were prepared by vapor-induced phase separation. Solutions were cast on glass substrate directly positioned inside a closed chamber. Relative humidity and temperature were set to $70 \pm 1\%$ and 30 ± 0.5 °C, respectively, one hour before starting membrane preparation, to ensure thermodynamic equilibrium inside the chamber. Polymeric solutions were exposed to water vapors during 20 min. Then, the newly formed films were immersed in a bath of DI water for 24 h, to remove all traces of solvent. Finally, membranes were dried directly on their substrate, at ambient temperature, and placing metal plates on each side of the films to avoid potential shrinkage during drying. Dried membranes were stored at 4 °C until use.

2.2.5. Physico-chemical characterization of casting solutions and of membranes

Two certified methods were used to determine the chemical composition of membrane surfaces. First, Fourier Transform Infra-Red (FT-IR) spectrophotometer was used. It was operated according to a method described elsewhere [6]. The C1s and O1s core-level spectra and the evolution of atomic composition were analyzed by X-ray Photoelectron Spectroscopy (XPS) according to a method also earlier reported [6].

A bioemission scanning electron microscope (SEM Hitachi S-4800, Japan) equipped with a Schottky field emission gun (10 kV), and with a cooling system (Eyela Cool ACE CA-1111) was used to characterize the morphology of the membranes. Images presented later were obtained from an accelerating voltage of 1 keV. Prior to introducing the samples in the SEM vacuum chamber, they were coated with a 1 nm gold layer using a sputter-coater model SC7620 metalizer.

Atomic distribution curve of cross section of one membrane cast from a solution containing 5 wt% copolymer was measured by energy dispersive (EDS) X-ray spectroscopy (Oxford Instruments, X max 80). Prior to analysis, samples were sputter-coated with Pt, and positioned in the SEM chamber of a JSM-7600F Schottky field emission scanning electron microscope (JEOL).

The surface roughness of membrane was determined with a JPK Instruments AG equipped with a Nanowizard XYZ scanner (Germany). The instrument was maintained in constant temperature using an AFM Zeiss Loop. Measurements were performed in acoustic alternating current air tapping mode. Image acquisition and processing were completed with a JPK Image Processing software associated to the AFM. Silicon cantilever probes (model NSC14/AIBS, length: $125\ \mu m \pm 5$, width: $35\ \mu m \pm 3$, thickness: $2\ \mu m \pm 0.5$) with a nominal resonant frequency between 110 and 220 kHz, and a force constant ranging between 1.85 and 12.5 N/m were used for sample scanning. Parameters such as the amplitude at which the cantilever probe oscillates, the typical scan rate and the scan area were adjusted.

The pore size and pore-size distribution were determined by capillary flow porometry (CFP-1500-AXEL, PMI), following a method earlier described [28]. The porosity of membranes was evaluated as follows: dry membrane samples (1.3-cm-diameter) were weighed and then immersed in ethanol (Aldrich) for 24 h. The excess of alcohol was gently wiped off the surface of the membranes, and samples weighed again. Then, we applied the formula available in literature leading to an evaluation of the porosity [29]. It has to be noted that it was previously checked that no removal of copolymer was observed over the duration of the test. In addition, the density of the copolymer was evaluated from the knowledge of the number of repeat units of each block and of the molecular weights of styrene and PEGMA repeat units.

Mechanical properties of membranes were evaluated by tensile tests measurements, performed with a DMA 7e instrument (Perkin-Elmer). The method used was similar to that employed earlier with PVDF/PS-*b*-PEGMA membranes [25].

The hydration properties of membranes were evaluated by determining their water contact angle and their hydration capability. Water contact angle of membranes was measured with an automatic contact angle meter (Kyowa Interface Science Co., Ltd. Japan) at ambient temperature (about 20 °C). DI water (4 μL) was dropped onto each sample and 11 pictures were shot over a 30-s-duration. Each picture was then analyzed to plot the evolution of WCA as a function of time. For each membrane, 7 independent kinetics were recorded, and the average reported. As for hydration capabilities of membranes (mg/cm^3), samples of a 0.85-cm-diameter and a pre-measured thickness were weighed with a 10^{-5} g precision balance and immersed into DI water for 24 h. Afterwards, superficial water was wiped out, and wet membranes weighed. The hydration capability was evaluated by taking the difference per cubic centimeter between the wet and the dry weights. Five independent measurements were done and the average taken as the membrane hydration capability.

2.2.6. Establishment of phase diagram and diffusion kinetics of non-solvent in casting solutions

Phase diagram was established at constant temperature $T = 70 \pm 1$ °C from the cloud point method. The choice of the temperature relies on the fact that Lin et al. mentioned gelation of PVDF solution at quite low temperature (50 °C) within a week [21]. Therefore, studying phase diagram at the same temperature used to prepare casting solutions (35 °C) would have made accurate conclusions difficult to draw, as gelation may occur before the onset of liquid/liquid demixing. Furthermore, the addition of water promotes gelation as well. Therefore, based on literature and preliminary tests, we chose to establish phase diagram 70 °C. To do this, a number of solutions with varying polymer initial concentrations were prepared. In order to study the effect of copolymer on thermodynamic stability of the casting solution and being able to draw accurate comparisons with the PVDF/NMP/water

ternary system, the PVDF/copolymer ratio was kept constant to 4:1. It enabled to represent in a same diagram the binodal curves of both the PVDF/NMP/water ternary system and of the PVDF/PEGMA$_{124}$-*b*-PS$_{54}$-*b*-PEGMA$_{124}$/NMP/water pseudo-ternary diagram. A quite similar approach has been reported by Mansourizadeh and Ismail who kept constant the additive to solvent ratio [30]. Once the solutions homogeneous, water was added drop wise under constant and vigorous stirring with magnetic bars (300 rpm). The addition of water led to local cloudy state indicating local demixing, but stirring enabled to regenerate the transparent state of the solution as water was homogeneously distributed in the entire volume. The cloud point was reached when cloudy state was permanent, despite a long (2 h) stirring. It was associated to the experimental binodal.

Kinetics of non-solvent transfer during phase separation was studied under the observation of optical microscope (Olympus microscope BX51TRF Model, Japan) with a magnification factor of $\times$ 10/0.25. A silicon wafer (thickness) was first positioned over a glass plate. Then, a tiny drop of polymer solution was placed on the silicon wafer and a glass microscope transparent slide pressed against the silicon wafer, allowing to spread the drop of polymer solution. Rhodamin B aqueous solution (23.5 mg in 10 g of DI water) was then introduced between the silicon wafer and the glass microscope slide and its diffusion recorded over time by a CCD color camera Toshiba and analyzed by Arc Soft webcam companion software. Water alone was not used in order to enhance the contrast and actually be able to follow the diffusion front of non-solvent. Therefore, it is assumed that the presence of dye does not significantly affect diffusion mechanisms of non-solvent.

Light transmission tests were performed at room temperature, according to the following experimental procedure. The coagulation bath was first filled up to 90% of its capacity with DI water, such that the stage would be completely immersed. A light source and a light collector were placed above and under the coagulation bath, respectively, and carefully aligned. The light sensor output value (without polymeric system) was about 1580 Lux, recorded with a light meter (DLM 536, Tecpel Co). After setting the system, the lights of the room were switched off, and the polymer solution cast on a glass plate with a metal casting knife such that the thickness was 300 μm (the same as that used to prepare membranes). The glass slide was immediately immersed in the coagulation bath, and small metallic plates were placed on the surface of the polymer film (at the top and at the bottom) to prevent the forming membrane from detaching from the plate and freely moving in the bath. Light transmission was continuously recorded until the light sensor output reached a stable value, indicating the end of phase separation.

2.2.7. Antibiofouling properties in static and dynamic conditions

Adsorption of bovine-serum-albumin and lysozyme (BSA, Mw $\approx$ 66,000 g mol^{-1}, Sigma® and LY, Mw = 14,300 g mol^{-1}, Sigma®) was studied according to a similar protocol. Membrane disks with a diameter of 1.3 cm were positioned in individual wells of a 24-well plate. A pretreatment with 1 mL of ethanol was first performed for 30 min, to allow swelling of matrices. Then, ethanol was replaced by a solution of phosphate-buffered saline (PBS). After 2 h in PBS at 25 °C, membranes were incubated with the solution of protein tested (either BSA or LY) at a concentration of 1 mg mL^{-1} and at 25 °C. Finally, in order to evaluate the amount of protein adsorbed onto and within the membrane, we measured the absorbance of the solution at 280 nm, using a UV–vis spectrophotometer (PowerWave XS, Biotech). Notice that before the measurement of absorbance, it was ensured that no tri-block copolymer was released over the duration of the adsorption test that would interfere with the determination of the absorbance.

As for fibrinogen (FN, Sigma®), the Enzyme-Linked ImmunoSorbent Assay (ELISA) procedure was followed. 3 Independent samples of each membrane were disposed in individual well of a 24-well plate containing PBS. The well-plate was then placed in an oven maintained at 37 °C, for 1 h. PBS was replaced by 1 mL of fibrinogen solution (1 mg/mL), and membranes incubated with the protein solution in an oven maintained at 37 °C. After a 2-h-incubation, membranes were rinsed using PBS, operation repeated twice, and then incubated in a BSA solution (1 mg/mL in PBS), at 37 °C for 1 h. Samples were thoroughly washed again with PBS, and soaked in a volume of 1 mL of primary monoclonal antibody (provided US Biological). Reaction was carried out at 37 °C for 30 min. After another triple washing with PBS, membranes were incubated with BSA at 37 °C for 1 h and then washed with PBS before adding 1 mL of horseradish peroxidase-conjugated secondary monoclonal antibody (1 mg/mL). After washing again the membranes 5 times with PBS, they were transferred into a clean well-plate, and incubated for 5 min at 37 °C with a 500 μL of solution at 1 mg mL-1 containing 3,3′,5,5′-tetramethylbenzidine chromogen 0.05 wt% Tween 20, and 0.05 wt% hydrogen peroxide. In order to stop the enzymatic reaction, 500 μL of sulfuric acid (0.1 M) were added. Eventually, a UV–vis spectrophotometer permitted to determine the absorbance at 450 nm of the solution, and then to evaluate the relative FN adsorption onto (and within) each membrane. The positive control (100% adsorption) was a polystyrene plate while the negative control was a poly sulfobetaine methacrylate hydrogel.

The anti-biofouling properties of membranes at the macroscale were also studied using (i) *Escherichia coli* modified with a green fluorescent protein, in order to facilitate observations of bacteria adhering onto the membranes and (ii) *Streptococcus mutans*. The procedure for genetic modification has been described elsewhere [31] while similar methods for culture and adhesion tests as those reported earlier for un-modified *E. coli* were adopted [6]. Therefore, one may want to refer to these works for further details.

To study the antibiofouling properties of membranes in dynamic conditions, cyclic-filtration tests were performed at 25 °C using a laboratory-scale unit (ADVANTEC®, Item LS-47-HP, Tokyo Roshi). The lab-scale cell is equipped with a tank containing the feed solution, a membrane module with an inner diameter of 20.5-mm, a nitrogen injection cylinder connected to the tank, a balance (MS8001 SE, Mettler Toledo) and a computer equipped with SerialPortToKeyboard software (METTLER TOLEDO). The membranes were positioned in the module on a macroporous stainless steel. In these tests, we used three types of microfiltration membranes:

- A PVDF, hydrophilic and bi-continuous ultrafiltration commercial membrane with an average pore-size of 0.1 μm (Millipore);
- A PVDF membrane (ID: P25-TB0) as-prepared by VIPS from the 25 wt% PVDF solution;
- A PVDF/PEGMA$_{124}$-*b*-PS$_{54}$-*b*-PEGMA$_{124}$ membrane (ID: P20-TB5) as-prepared by VIPS from the solution containing 25 wt% PVDF and 5 wt% PEGMA$_{124}$-*b*-PS$_{54}$-*b*-PEGMA$_{124}$.

Before each filtration experiment, membranes were immersed in ethanol (50% v/v) for 15 min, and permeability was controlled initially by filtering DI water. The permeate flux was quantified by measuring continuously the weight of permeate by the mean of an electronic balance. Cyclic filtrations were performed according to the following experimental procedure. An over pressure (1.5 atm) water cycle was ran for 30 min to compact the membrane system. Then, pressure was decreased to 1 atm, and water permeate flux recorded for 1 h ($J_{w,0}$). Thereafter, a BSA solution in PBS (1 g/L) was filtrated through the membrane at play for 1 h ($J_{BSA,1}$). Membranes were then washed by flushing them with DI water and then

performing a DI backflushing cycle for 30 min in DI water. This operation allowed removing reversible fouling (cake layer). Subsequently two other water-BSA cycles (30 min – 1 h) were run similarly, and the test was ended by a last water cycle. Following filtration tests, we determined the global flux recovery ratio ($FRR_G = (J_{w,3}/J_{w,0}) \times 100\%$), the flux recovery ratio after each cycle ($FRR_i = (J_{w,i}/J_{w,i-1}) \times 100\%$, $i=1,2,3$), the global irreversible flux decline ratio ($DR_{ir,G} = [(J_{w,0} - J_{w,3})/J_{w,0}] \times 100\%$) and the irreversible flux decline ratio after each cycle ($DR_{ir,i} = [(J_{w,i-1} - J_{w,i})/J_{w,i-1}] \times 100\%$, $i=1,2,3$).

3. Results and discussion

3.1. Molecular structure of tri-block copolymer

The characteristic ^{1}H NMR spectrum of the tri-block copolymer is shown in Fig. 1. The exact composition, in terms of number of hydrophobic and hydrophilic blocks, can be assessed using the proton resonance of the aromatic group of PS block (chemical shift δ at 7.08, 7.13 and 7.18 ppm for protons *g*, *g′* and *g″*, respectively), and that of the protons *d* of the methoxyl group constituting the PEGMA side block ($\delta = 3.24$ ppm). According to the ^{1}H NMR spectrum, the ratio of the area of the signals of the five aromatic protons to that of the signal of the six protons carried by the methoxyl groups ($H_{g-g''}/H_d$) was found to be 0.36. Therefore, from the knowledge of the molecular weight of the tri-block copolymer, found to be 29,850 g/mol by GPC analysis, and that of each repeat unit, it could be concluded that the number of anchor hydrophobic group was 54 while 248 repeat units constituted the hydrophilic blocks of the copolymer. In sum, we obtained the following copolymer: $PEGMA_{124}$-*b*-PS_{54}-*b*-$PEGMA_{124}$.

3.2. Physicochemical characterization of membranes: membrane formation aspects

SEM images of PEGylated PVDF membrane surfaces and cross-sections are shown in Fig. 2 while AFM images are displayed in Fig. 3. In general, we observed that the structure of membranes was mostly composed of interconnected domains characteristics from lacy structure, with some very small spherulites or nodules dispersed in the matrix. Nodule formation arises from crystallization, and was shown to strongly depend on the temperature of dissolution of the casting solution in the work of Lin et al. using

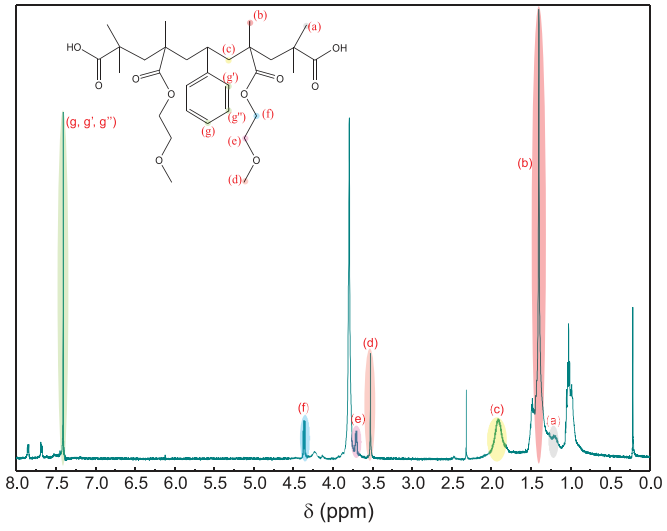

Fig. 1. H^{1}NMR of $PEGMA_{124}$-*b*-PS_{54}-*b*-$PEGMA_{124}$ tri-block copolymer.

octanol as a non-solvent [26]. Later, Li et al. studied the formation of PVDF membranes by VIPS, from casting solutions containing 20 wt% polymer, and also unveiled that below a certain temperature (32 °C in their case), mechanism for membrane formation was a non-crystallization gelling process [27]. Arising structure was lacy, with interconnected polymer-poor and polymer-rich domains. But the critical dissolution temperature depends on the solvent, the nature of the polymer and on its molecular weight, as well as it might be affected by the concentration, and on the system at play. Here, we used a different PVDF at a different concentration and blended with a tri-block copolymer, so that parameters controlling structure formation must be different. We chose 35 °C as the dissolution temperature because the casting solutions all contained 25 wt% total dry matter. Their viscosity was therefore quite high (results are shown in Table 1) and prevented us to obtain homogeneous solutions in a reasonable amount of time. It seems however that this temperature is in the region of the critical dissolution temperature since interconnected domains with small nodules were formed.

The formation of this so-called mix-structure can be further supported by the analysis of the FT-IR spectra in the lower region of wavenumbers. If nodules are mostly formed, then there are associated with the dominating β-polymorph which stretching band can be found at 840 cm^{-1} for instance [32]. On the other hand, α-polymorphs (stretching band at 763 cm^{-1}) dominate in lacy structures [27]. Here, both polymorphs are found (Fig. 4). However, the calculus of the mass fraction of the α-form in the crystal according to the equation reported by Li et al. leads to a value ranging between 56.5% and 59.8%, which is pretty high and suggests that the structure arises mostly from a non-crystallization gelling process [27]. In addition, it is worth noting that the overall crystallinity of the membranes tended to remain almost unchanged (Fig. S2 and Table S1).

Furthermore, there is visually not much effect of the copolymer on membrane formation aspects even if the nodules size seems to slightly decrease with copolymer content, which would suggest that crystallization is further hindered. We conducted non-solvent diffusional tests and determined the phase diagrams to get insights into the thermodynamic aspect of membrane formation. It is also important to insist on the fact that the viscosity of the PEGylated solutions decreases as the copolymer content increases, as shown in Table 1. This implies that viscous forces preventing non-solvent penetration are not as strong for the PVDF/$PEGMA_{124}$-*b*-PS_{54}-*b*-$PEGMA_{124}$/NMP system than they are for the PVDF/NMP system (physical effect). Consequently, the penetration of water is expected to be facilitated. Also, as the copolymer is amphiphilic, it is believed to promote water diffusion and thus the onset of phase separation (chemical effect). This can be seen on the diffusion kinetics of water as a function of the copolymer concentration plotted in Fig. 5a. Clearly, the distance travelled by water in a given amount of time is longer as the concentration of $PEGMA_{124}$-*b*-PS_{54}-*b*-$PEGMA_{124}$ increases. Diffusion coefficients of water in the polymeric system can be compared by plotting the distance travelled by water in the system as a function of the square root of time (Fig. 5b), assuming 2D diffusion. The slope of the initial linear portion enables to determine $D_{w/m}$. Doing so, diffusion coefficients of water in a solution containing no copolymer (virgin), 1 wt% copolymer, 3 wt% copolymer and 5 wt% copolymer were found to be 9.51×10^{-11} m^2/s, 1.03×10^{-10} m^2/s, 1.42×10^{-10} m^2/s and 1.76×10^{-10} m^2/s, respectively. This fast exchange is further supported by light transmission tests (Fig. 6), unveiling that a change of light transmission occurs earlier in the case of PVDF/$PEGMA_{124}$-*b*-PS_{54}-*b*-$PEGMA_{124}$/NMP, meaning that membrane formation happens faster than in the system without additive. Fast diffusion is not favorable to the growth of nodules, arising from crystallization which is kinetically slower than non-

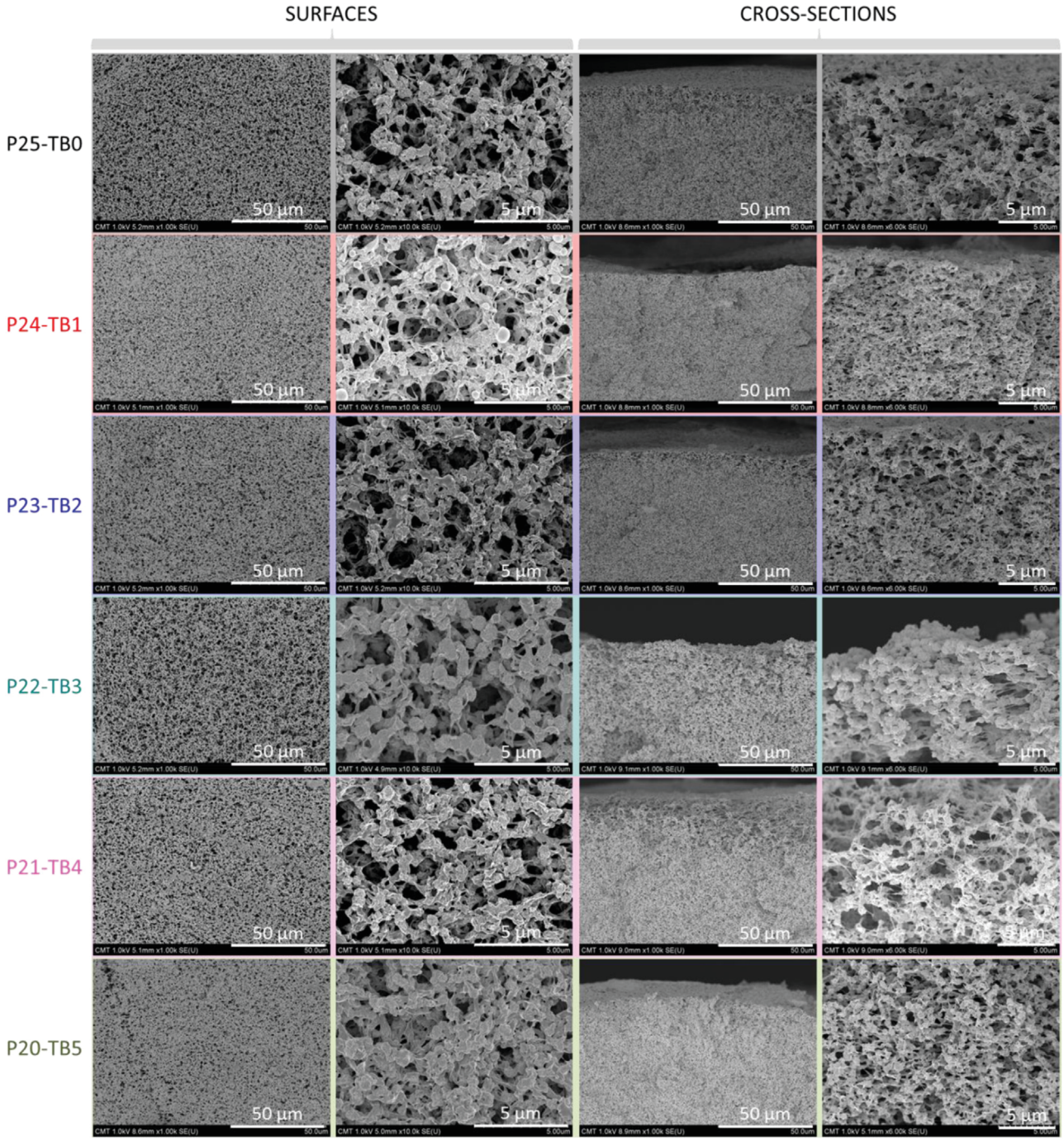

Fig. 2. Morphological characterization of virgin and PEGylated PVDF membranes by scanning electron microscope.

crystallization gelling processes [32]. Additionally, it appears that the PVDF/PEGMA$_{124}$-*b*-PS$_{54}$-*b*-PEGMA$_{124}$/NMP ternary system is not as thermodynamically stable as the PVDF/NMP binary system, as the pseudo-ternary diagram reveals that the binodal is slightly shifted toward the solvent/polymer axis (Fig. 7). This implies that less water is necessary to induce phase-separation and to cross the metastable region in which metastable domains could still grow. It is again not favorable to the formation of crystalline nodules. All these evidences explain the dominance of interconnected polymer domains with only a few nodules.

Finally, as there was no major change of morphology observed, it seemed reasonable to obtain roughness coefficient (marked on Fig. 3), bubble point pore diameters and porosity in the same range (Table 2). All membranes can be applied in the MF range as they exhibit large pores and a high surface porosity (76–80%). Nonetheless, characterization results of mechanical properties tend to show that the PVDF/PEGMA$_{124}$-*b*-PS$_{54}$-*b*-PEGMA$_{124}$ are somewhat stronger than virgin PVDF membrane (Table 2 and Fig. S3 in Supporting information section). Indeed, we measured a modulus of elasticity in tensile mode of 87 ± 14 MPa for virgin PVDF membrane, while it was found to be 133 ± 4 MPa for P20-TB5 membrane. In addition, the tensile stress at break was 0.81 ± 0.10 MPa for virgin PVDF membrane and increased up to 1.54 ± 0.09 MPa for P20-TB5. These results support that modified membranes are slightly stronger and stiffer than virgin PVDF membrane. However, ductility of P20-TB5 was less than that of virgin membrane ($2.92 \pm 0.34\%$ *vs.* $9.03 \pm 2.62\%$) but no clear trend was really identified for the elongation at break as it increased and

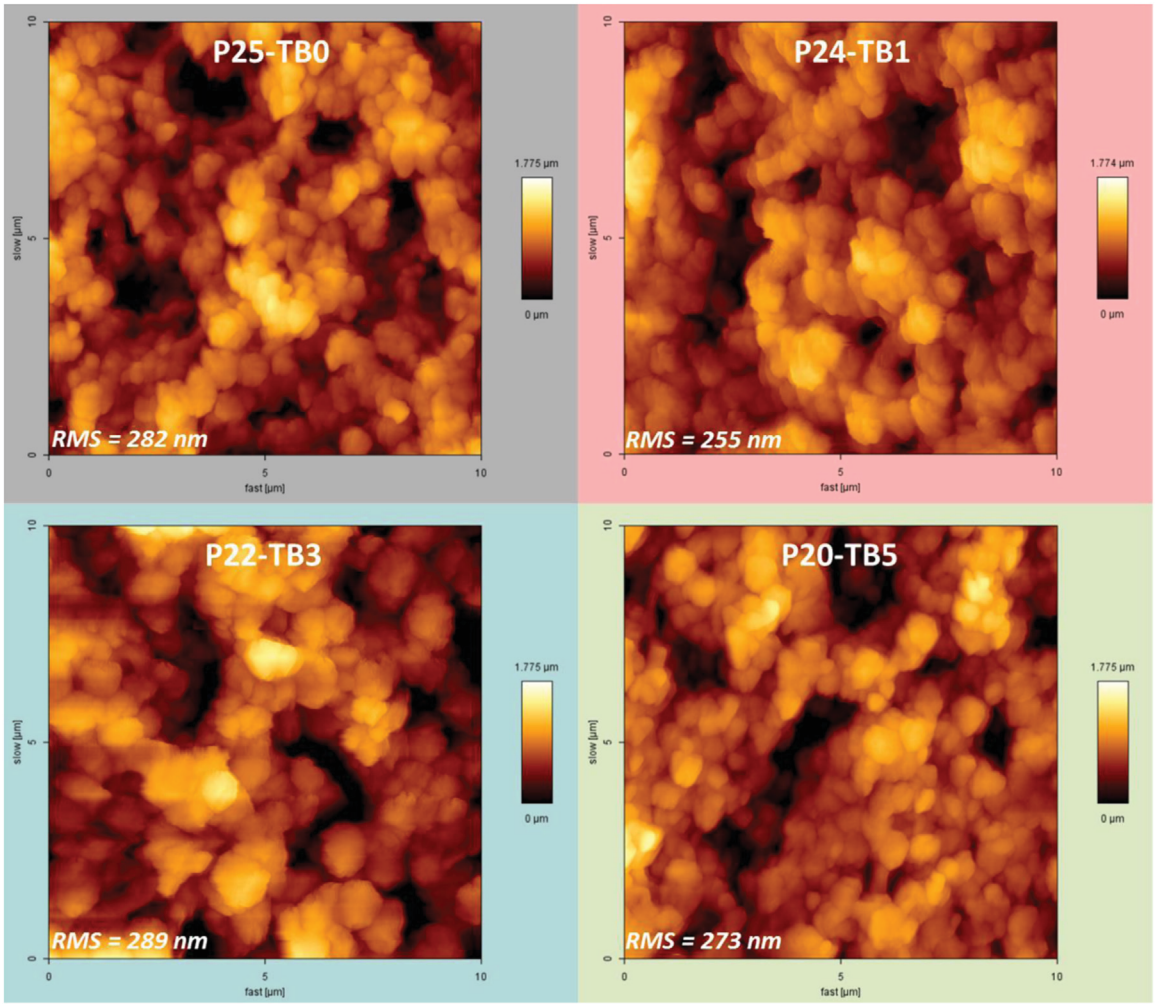

Fig. 3. Morphological characterization of virgin and PEGylated PVDF membranes by atomic force microscope.

then decreased with the polymer content. Finally, the trends observed for modulus of elasticity and tensile stress at break also revealed that the entanglement between polymer domains is quite strong for modified membranes, and so, that crystallization played a minor role on the formation of these membranes.

Regarding the chemical properties of the surfaces, FT-IR characterization confirms that $PEGMA_{124}$-*b*-PS_{54}-*b*-$PEGMA_{124}$ is present at the surface of membranes (Fig. 4). Besides the different crystalline polymorphs evidenced in the finger print region and above-discussed, FT-IR analysis reveals the presence of absorption bands at 1729 cm^{-1} and 1100 cm^{-1}, assigned to the –C=O and –C–O stretching vibrations of carbonyl group and carboxylic ester, respectively. This band was still clearly visible after 6 weeks immersion in DI water, supporting the stability of the system (Fig. S4 in Supporting information section). The signal observed at 2871 cm^{-1} are ascribed to the stretching and bending vibrations of methylene ($–CH_2$) carried by PEGMA hydrophilic heads. The intensity of all these peaks revealing the presence of the triblock copolymer tended to increase with additive concentration. Furthermore, as clearly seen on the O1s core-level spectra (Fig. 8a) as well as on the plot presenting the element content as a function of copolymer content in the initial casting solution (Fig. 8b), XPS analysis did evidence a significant increase of oxygen content at the surface of membranes from a 2 wt% $PEGMA_{124}$-*b*-PS_{54}-*b*-$PEGMA_{124}$ content, which also supports the presence of copolymer at the surface of the membranes. Finally, the EDS analysis performed on P20-TB5 membrane and presented in Fig. 9 shows that the oxygen signal recorded along the cross-section tends to fluctuate around a mean value, which implies that the copolymer is dispersed within the membrane. In other words, this analysis reveals that not much migration of copolymer toward the upper surface occurred during membrane formation, as it could have been expected considering the relative slowness of mass transfer rates involved in VIPS, but further investigations are needed to clarify this point.

Taken all together, characterization results suggest that membranes are physically and chemically homogeneous, and PVDF membranes have been modified in a relatively controlled fashion. The next question is related to whether the surface and bulk-modification of the PVDF membrane by the tri-block copolymer enables to trap water and lead to low-fouling properties.

3.3. Resistance of PEGylated membranes to biofouling in static conditions

3.3.1. Effect of tri-block copolymer on hydration properties of membranes

A first acknowledged step toward the development of non-fouling membranes is the design of a hydrophilic protective layer at the surface and within the pores, that will prevent foulants to stick on and within the matrix. Hydrophilicity of the membrane is therefore critical, and in particular its ability to trap water, which is evaluated through the measurement of the hydration capacity, reported in unit mass of water trapped per unit volume of

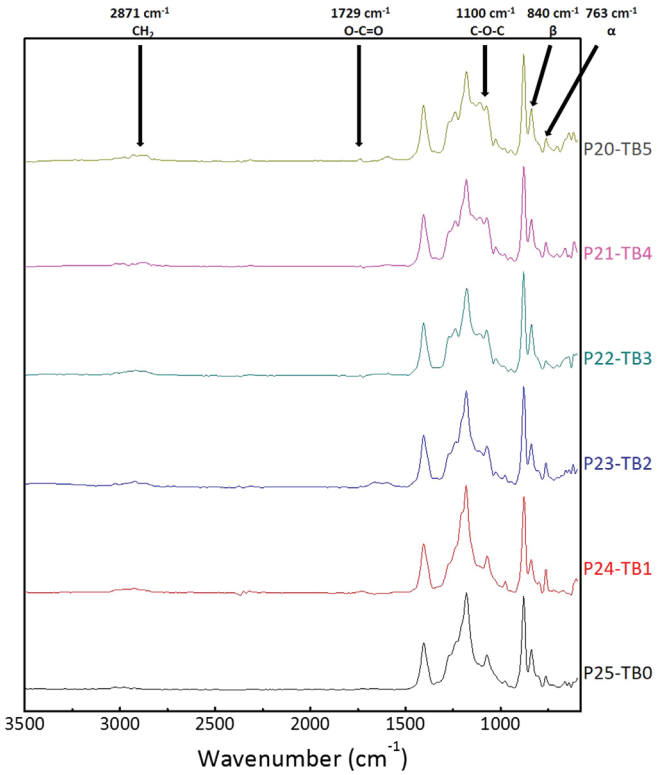

Fig. 4. Chemical characterization of membranes surface by FT-IR spectroscopy.

membrane. We noticed in preliminary tests that the WCA of membranes containing the highest content tested of block copolymers was slightly changing over a 30-s-time period, probably due to the wetting of the surface pores, but the change is not obvious on other membranes: a decrease of 3% and 8%, as compared to the initial data of water contact angle for P21-TB4 and P20-TB5, respectively, was measured over the duration of analysis (Fig. S5 in the Supporting information section). Clearly, the addition of block copolymer allows increasing the surface hydrophilicity of the membrane, as the WCA decreases from about 126° to 109° (Fig. 10). Values are still high, ascribed to the very rough and porous structures obtained in each case, but for membranes modified with triblock, hydration did occur, arising in a slight decrease of WCA. The overall ability of the

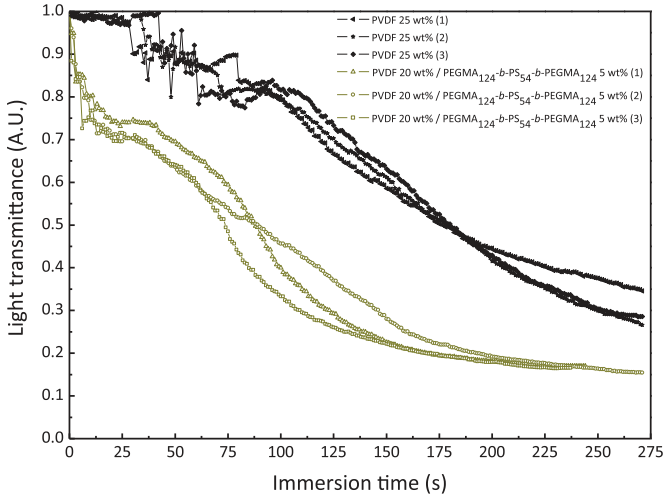

Fig. 6. Light transmission curves.

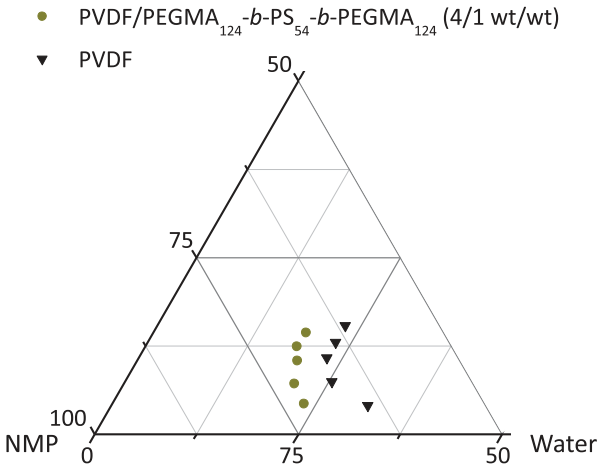

Fig. 7. Effect of $PEGMA_{124}$-*b*-PS_{54}-*b*-$PEGMA_{124}$ tri-block copolymer on thermodynamic stability of the casting solution at 70 °C.

$PVDF/PEGMA_{124}$-*b*-PS_{54}-*b*-$PEGMA_{124}$ membranes to trap water is then clearly seen on the plot reporting their hydration capacity. Obviously, when contacted with water or hydrophilic solution for a long period of time (24 h in the present case) like during filtration,

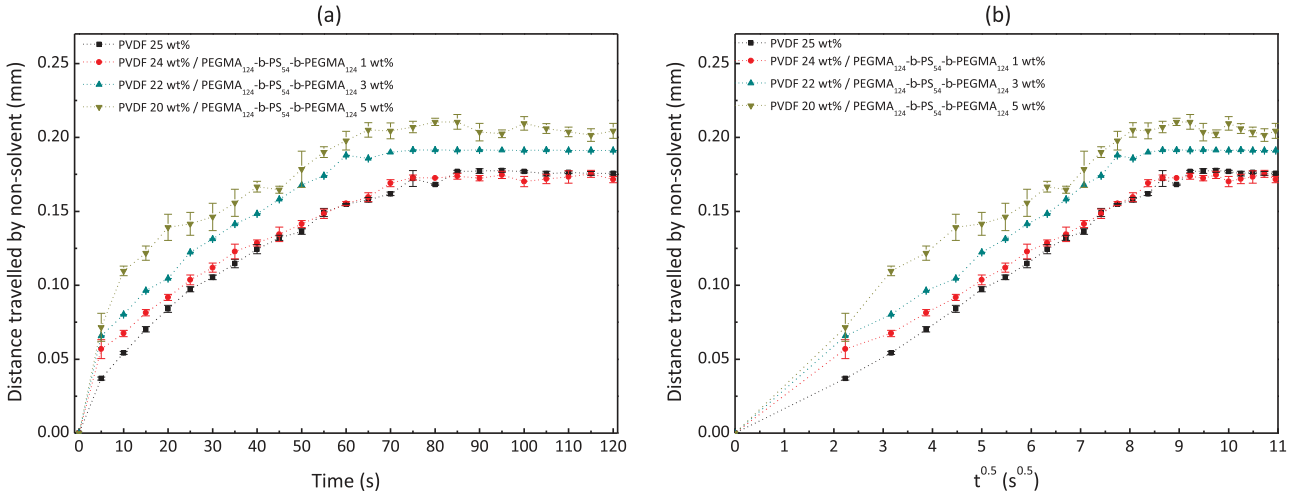

Fig. 5. Effect of $PEGMA_{124}$-*b*-PS_{54}-*b*-$PEGMA_{124}$ tri-block copolymer on diffusion rate of non-solvent in the casting solution. (a) Diffusion kinetics plotted from microscope images; (b) distance travelled by non-solvent as a function of the square root of time: assessment of diffusion coefficients.

Table 2
Characterization of porous-structure and mechanical properties of virgin and PEGylated membranes.

Membrane ID	Bubble point pore diameter (μm)	Porosity (%)	Thickness (μm)	Tensile stress at break (MPa)	Modulus of elasticity (MPa)	Elongation at break (%)
P25-TB0	0.25	80.1 ± 1.7	106 ± 1	0.81 ± 0.10	87 ± 14	9.03 ± 2.62
P24-TB1	0.44	84.1 ± 2.2	111 ± 6	0.72 ± 0.07	76 ± 11	17.92 ± 0.42
P23-TB2	0.43	80.3 ± 0.2	103 ± 2	0.83 ± 0.02	76 ± 2	10.51 ± 0.80
P22-TB3	0.31	80.1 ± 0.7	104 ± 4	0.98 ± 0.12	91 ± 16	9.31 ± 0.83
P21-TB4	0.33	80.2 ± 3.5	115 ± 4	1.17 ± 0.22	114 ± 30	19.21 ± 8.96
P20-TB5	0.31	76.5 ± 2.1	116 ± 2	1.54 ± 0.09	133 ± 4	2.92 ± 0.34

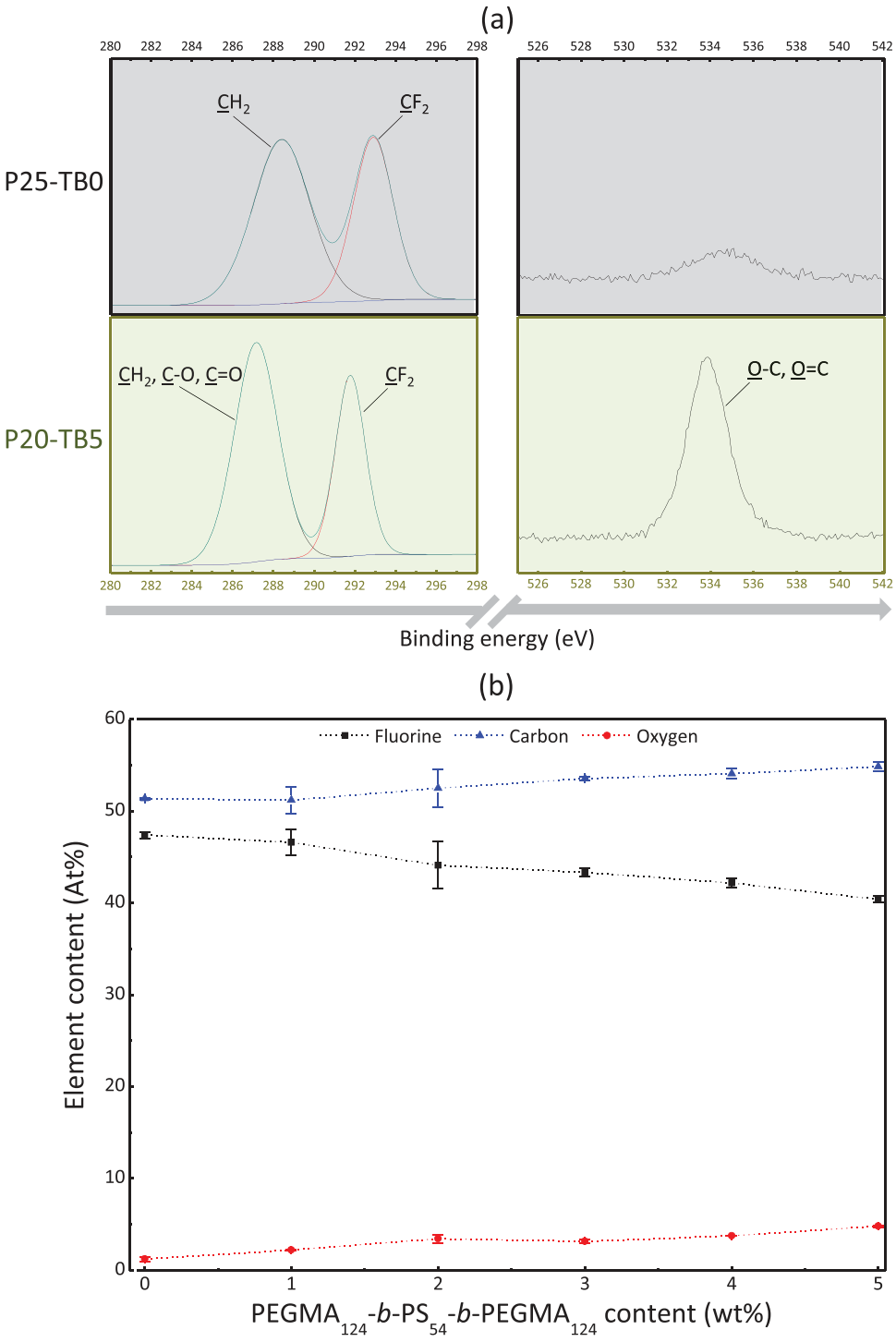

Fig. 8. Chemical characterization of membranes surface by XPS spectroscopy. (a) C1s core-level spectra of P25-TB0 (virgin PVDF) and P20-TB5 (PEGylated PVDF) membranes verifier bandes; (b) element content analysis.

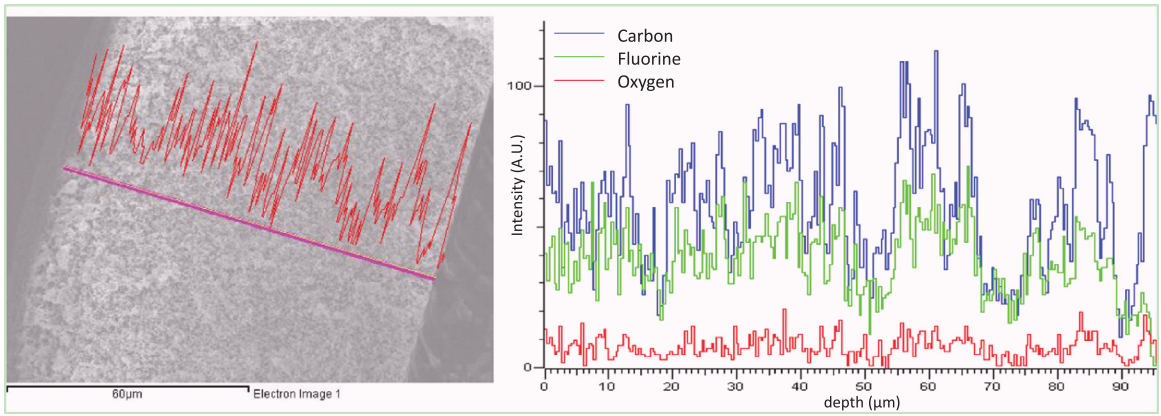

Fig. 9. Energy dispersive spectroscopy analysis of P20-TB5 membrane.

water is trapped by the PEGylated chains dispersed all over the membrane thickness (Fig. 9b). This yields to a dramatic improvement of hydration capacity from about 59 mg/cm^3 to 650 mg/cm^3. The value reported here should be challenged against those reported in literature, but most of the time, researchers report values per unit surface area, as surface-modification are mostly performed, which prevented us to draw accurate comparisons. A plateau tends to be reach from a 4 wt% copolymer content, which indicates that the bulk tends to be saturated with hydrophilic PEGMA moieties.

3.3.2. *Effect of tri-block copolymer on resistance to nonspecific protein adsorption*

Once the ability of membranes to bind water verified, we investigated the adsorption of BSA, LY and FN, model proteins often used to evaluate the nonfouling properties of membranes to be applied in water treatment, waste water treatment or blood filtration [33–38]. Starting with, BSA, this is a globular protein which non-polar residues facilitate hydrophobic–hydrophobic interactions, eventually leading to biofouling at the nanoscale. Results presented in Fig. 11 reveal that the block copolymer clearly acts as a fouling-resistant agent. If the virgin PVDF membrane exhibits an adsorption level of 0.19 ± 0.02 mg/cm^2 (normalized to 100%), this value is decreased up to 90% for P20-TB5 membrane. One will notice that this result is quite remarkable, given the porous structure of the membrane and its roughness, enabling to physically trap biofoulants. As expected, relative protein adsorption decreases with additive content, whatever the protein studied, unveiling the efficiency of the additive to resist non-specific protein adsorption. From a 3 wt% additive content, the adsorption of lysozyme was less than 20% that of the virgin PVDF membrane and decreased to 15% from 4 wt% copolymer. Similar excellent resistance is obtained when the protein is fibrinogen, with adsorption decreased to 90%. Fibrinogen is a larger protein and therefore contains more adsorption sites than BSA and LY. Its adsorption is a major issue in particular when membranes are to be used in plasma or blood filtration, as it then mediates the adsorption and activation of cells, leading to clotting and so, further increases biofouling [39,40]. It appears that membranes prepared in this study resist non-specific adsorption of proteins and also in particular model blood plasma protein, such that their application could be oriented toward either water treatment or blood filtration.

Finally, as noted in section 3.2.1, from a 4 wt% additive content, optimal resistance to biofouling by protein was reached, as the matrix was saturated with water. Not much improvement was therefore measured when comparing P21-TB4 and P20-TB5.

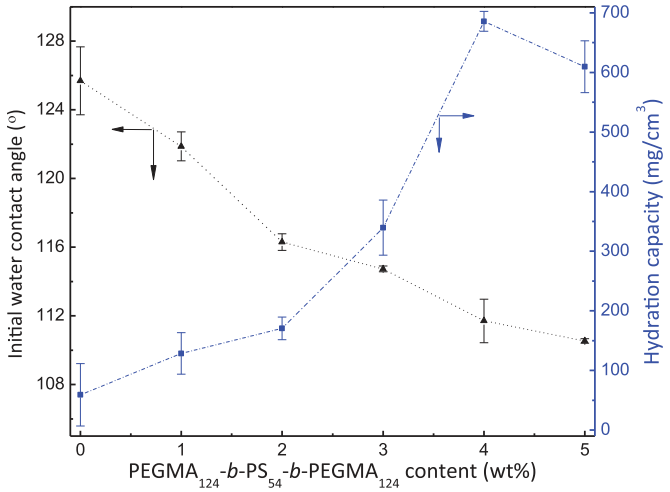

Fig. 10. Hydration properties of virgin and PVDF/PEGMA$_{124}$-*b*-PS$_{54}$-*b*-PEGMA$_{124}$ membranes.

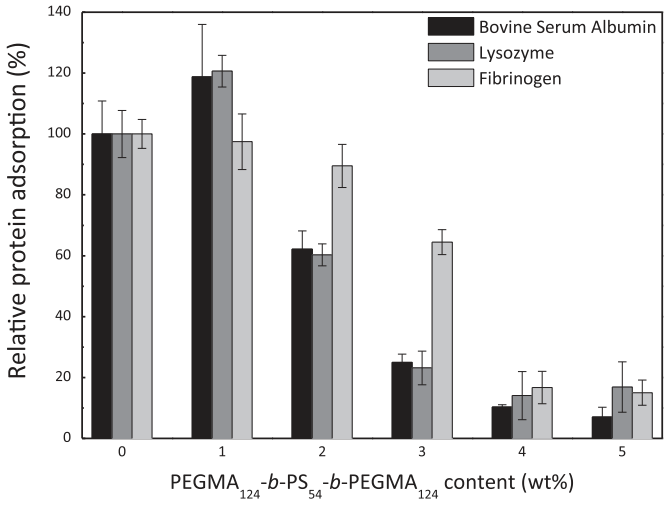

Fig. 11. Effect of PEGMA$_{124}$-*b*-PS$_{54}$-*b*-PEGMA$_{124}$ tri-block copolymer on resistance to nonspecific protein adsorption.

3.3.3. *Effect of tri-block copolymer on resistance to bacterial attachment*

Alike for protein adhesion, bacterial attachment is affected by both the physical state of the interface and its chemistry. For microfiltration membranes, bacterial species can be easily trapped within the pores, and even squeeze through smaller pores as some

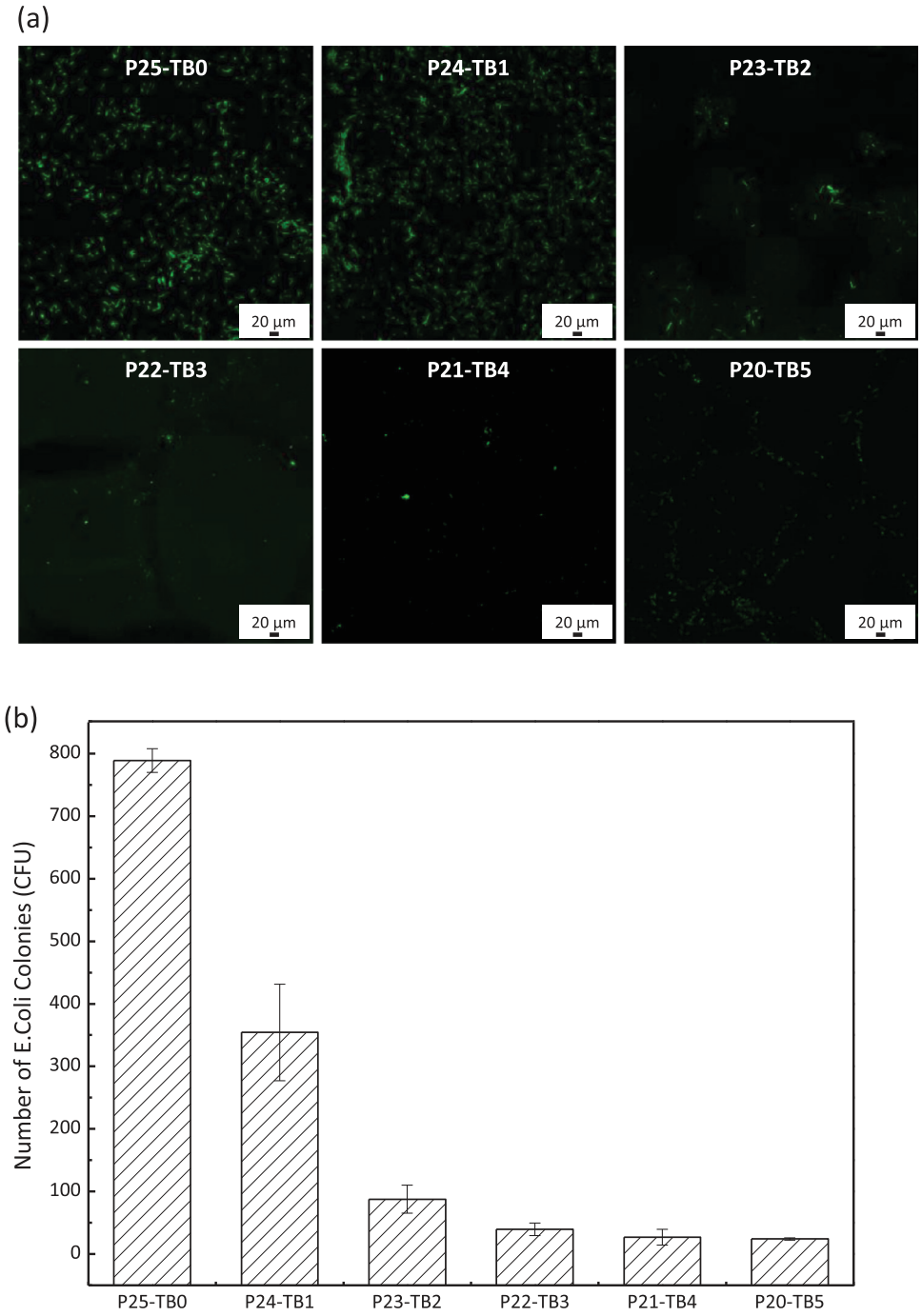

Fig. 12. Effect of $PEGMA_{124}$-*b*-PS_{54}-*b*-$PEGMA_{124}$ tri-block copolymer on resistance to *E. coli* attachment. (a) Confocal analysis; (b) quantitative analysis obtained from confocal images.

have a deformable cell-wall [41]. In this respect, finely tuning the chemistry of the interface is critical. We have seen from previous hydration and protein adsorption results that a plateau tended to be reached from a 4 wt% copolymer content (in the initial casting solution). This would indicate that the interface is saturated with nonfouling moieties and should therefore offer a protective barrier to bacterial invasion. In order to check the ability of our engineered membranes to resist bacterial attachment, we performed bacterial adhesion tests using *E. coli* as a model protein, a deformable micro-organism commonly employed in studies on the development of antifouling membranes. We modified it with a green-fluorescent protein to facilitate observation. In addition, we tested a gram-positive bacteria, *S. mutans* to have a wider overview of the actual nonfouling properties of our membranes. Results presented in Figs. 12 and 13 indicate that many species interact with the virgin PVDF matrix, given its hydrophobicity and its physical nature. For membranes prepared from casting solutions containing between 1 to 3 wt% copolymer, many green spots are still observed on related confocal images. Although they are more hydrophilic, these membranes do not present a copolymer concentration high enough to efficiently prevent the approach of bacteria and repel them. Additionally, their quite high roughness characteristic from such structure (Fig. 3) also contributes to bacterial entrapment and adhesion between small nodules. This is

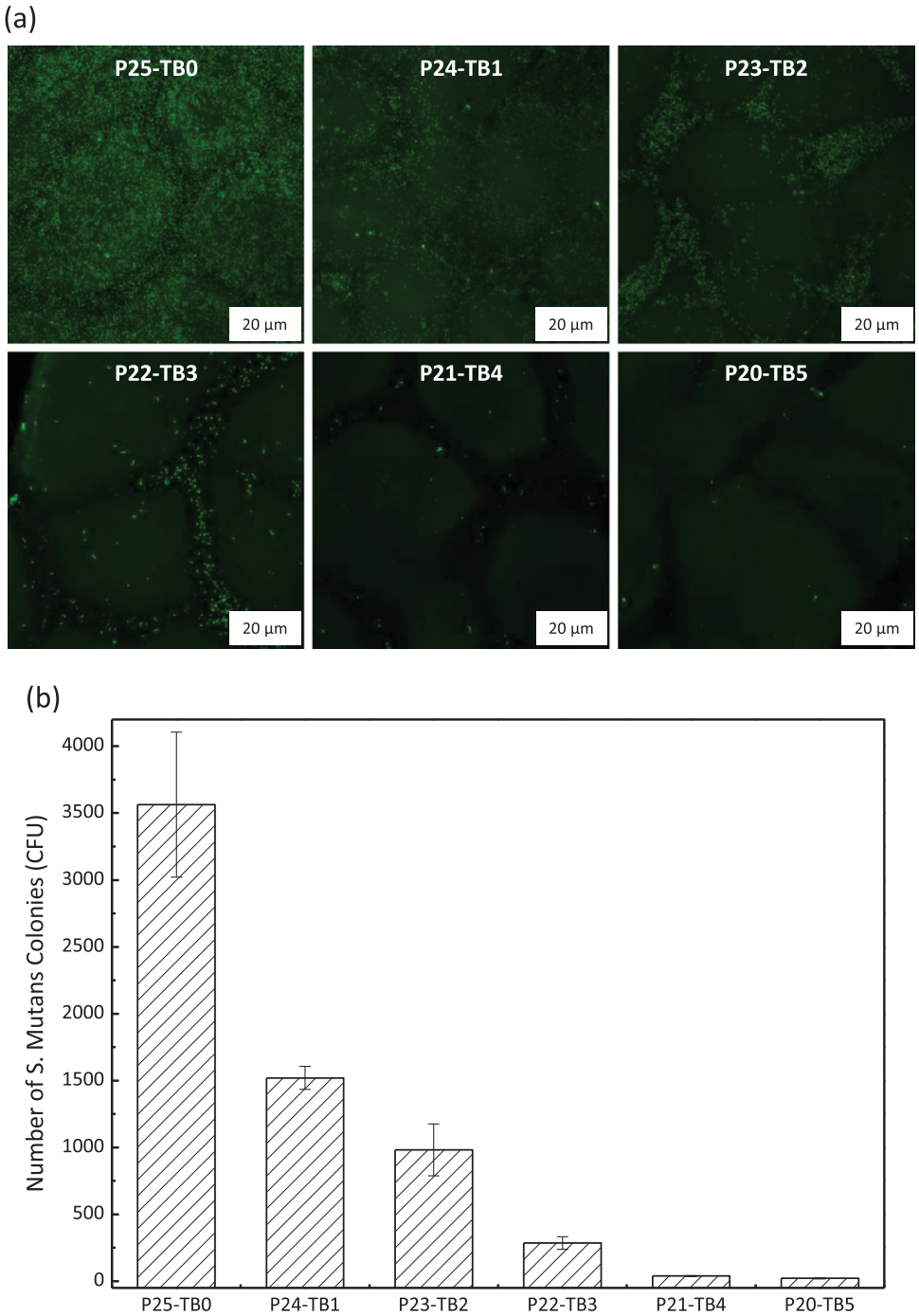

Fig. 13. Effect of $PEGMA_{124}$-*b*-PS_{54}-*b*-$PEGMA_{124}$ tri-block copolymer on resistance to *S. mutans* attachment. (a) Confocal analysis; (b) quantitative analysis obtained from confocal images.

also interesting to notice that the extent of adhesion is strongly dependent on the nature of the bacteria species, that is, different cell-walls interact differently with the membrane material at play. Hence, more than 2300 CFU were counted on confocal observation of virgin membranes for *S. mutans* tests, while there were less than 800 CFU in *E. coli* tests. This implies that global resistance to bacteria species is not readily achieved. Yet, as almost no bacteria can be found onto membranes containing the highest copolymer concentrations (P21-TB04 and P20-TB5), it can be concluded that the copolymer used offers a high protection toward bacterial attachment and that the membranes are nonfouling at the microscale.

3.4. Resistance of PEGylated membranes to biofouling in dynamic conditions

We can reasonably state that in static conditions, polymer chains are not deformed as they would be under the stress of a drag flow, as in filtration. Deformability of antifouling moieties and spatial rearrangement can severely affect the extent of biofouling, such that resistance to biofouling in dynamic conditions has to be assessed too. Therefore, filtration tests were run, using BSA in standard conditions [42,43]. Here, we compared the performances of the most PEGylated membrane (P20-TB5) to that of the virgin membrane (P25-TB0) and of a commercial hydrophilic PVDF microfiltration membrane (Millipore®).

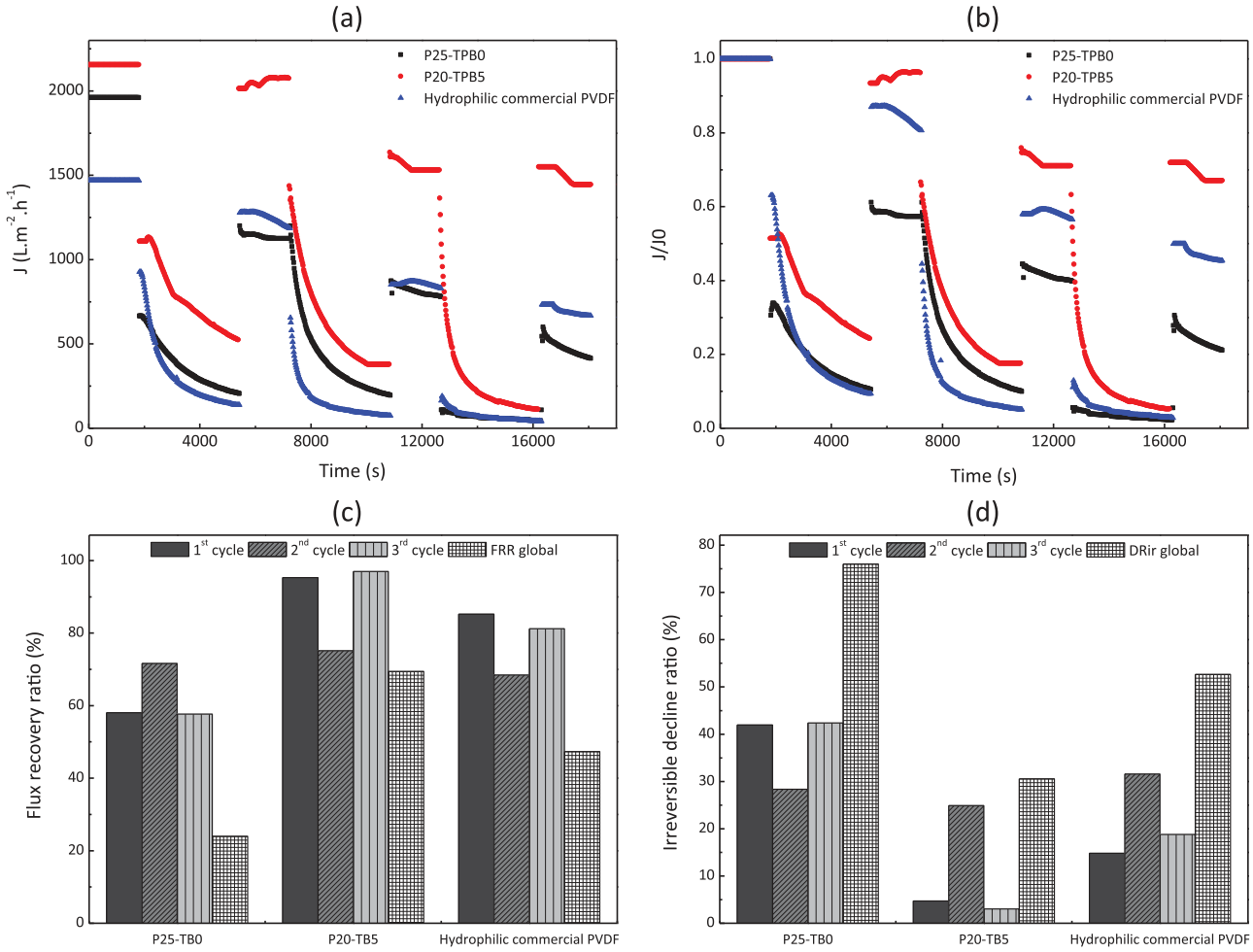

Fig. 14. Effect of $PEGMA_{124}$-*b*-PS_{54}-*b*-$PEGMA_{124}$ tri-block copolymer on resistance to biofouling by BSA protein during filtration. (a) Flux over filtration time; (b) dimensionless flux over filtration time; (c) evaluation of flux recovery ratios; (d) evaluation of irreversible flux decline ratios.

Results reported in Fig. 14 unveil a typical important flux decline due to interactions of membrane material with biofoulants, for both virgin PVDF membrane and hydrophilic commercial PVDF membrane. The global FRR (calculated by taking into account initial water permeability and that after the very last cycle) were found to be 24.0% and 47.3% for virgin PVDF and commercial hydrophilic PVDF membrane, respectively. Reversible biofouling and pore clogging of membranes both occurred. However, for the membrane modified with the tri-block copolymer, if a permeability decline was still observed, it was not as important as with the other membranes after each filtration cycle with FRR found to be 95.3%, 75.1% and 97.0.% after cycle 1, 2 and 3, respectively, thus corresponding to a global FRR of 69.4%. This promising result was logically attributed to the nonfouling effect of $PEGMA_{124}$-*b*-PS_{54}-*b*-$PEGMA_{124}$. This difference in flux recovery is even better highlighted in Fig. 13b as after 3 cycles, the dimensionless water fluxes obtained with virgin PVDF membrane and commercial hydrophilic PVDF membrane are importantly lower than that obtained with the PVDF/$PEGMA_{124}$-*b*-PS_{54}-*b*-$PEGMA_{124}$ membrane. Moreover, we measured an important decreasing of irreversible flux decline ratio with the modified membrane (Fig. 13d), meaning that fouling of P20-TB5 membranes is mostly reversible, which somewhat better reveals the efficiency of $PEGMA_{124}$-*b*-PS_{54}-*b*-$PEGMA_{124}$ as a low-biofouling material for *in-situ* modification of PVDF membranes.

Our results on the low-biofouling properties of P20-TB5 membrane during filtration can be compared with those of literature. Water flux recovery ratios obtained after filtration of a BSA solution were reported to be 73%, 78.2%, 81.2% and 83%, that is slightly higher than in the present study, with antifouling PVDF membranes prepared by blending PVDF polymer with PVDF-*g*-PVP [3], poly(methyl methacrylate-2-hydroxyethyethyl metacrylate-acrylic acid) [44], PVDF-*g*-PSMA [45], and cellulose acetate [46]. However, we performed three filtration cycles, unlike Xu et al. [3], Ju et al. [44], Li et al. [45] or Razzaghi et al. [46] who only performed one or two filtration cycles. Our FRR after one cycle is comparable to that obtained by Abed et al. with PVDF-*g*-POEM but they designed hollow-fiber membranes so that accurate comparisons cannot really be made [47]. In addition the P20-TB5 membrane generates a lower irreversible fouling ratio than the best one reported by Bera et al. in their report on antifouling PVDF membranes prepared from blends [48].

4. Conclusions

In this work, we presented a novel triblock copolymer, made of one anchor block of poly(styrene) and two blocks of poly(ethylene glycol) methacrylate hydrophilic moieties. We then used this triblock copolymer in blend with PVDF in order to prepare low-biofouling membranes by vapor-induced phase separation. A number of significant results were highlighted:

1. At the dissolving temperature chosen, PVDF membranes are close to be bi-continuous structure. The formulation was such that the copolymer promoted diffusion rate of non-solvent (chemical

effect inherent to the hydrophilic nature and physical effect due to a decreasing of viscosity). Combined to a lesser thermodynamic stability, crystallization had even less chance to occur, favoring the formation of PVDF/PEGMA$_{124}$-*b*-PS$_{54}$-*b*-PEGMA$_{124}$ membranes by non-crystallization gelling process, leading to bicontinuous structures.

2. The copolymer is well distributed over the whole matrix and remains in the system after phase separation, leading to greatly improved hydration properties of the membranes.
3. Biofouling in static (BSA, LY and FN adsorption, *E. coli, S. mutans* attachment) and dynamic conditions (BSA-water filtration cycles) was importantly inhibited. In particular, the adsorption of proteins was reduced to 85–90%, depending on the nature of the proteins, and global FRR after 3 BSA-water cycles was 69.4%, value much higher than that obtained with commercial membrane (47.3%).

All these results suggest that these novel MF membranes could be used in water-treatment applications (MBR). In addition, the assessment of hemocompatible properties of these novel membranes is on-going, given the very good resistance to fibrinogen measured.

Acknowledgments

The authors express their sincere gratitude to the Ministry of Science and Technology for their financial support through the Grant MOST 104-2221-E-033-066-MY3. This study was also partly funded through a joint program between the Ministry of Science and Technology (MOST, former National Science Council of Taiwan) and the Agence Nationale de la Recherche (NSC-ANR Blanc International II Program: NSC 103-2221-E-033-074 and ANR-12-IS08-0002).

Appendix A. Supplementary material

Supplementary data associated with this article can be found in the online version at http://dx.doi.org/10.1016/j.memsci.2016.03.017.

References

[1] D. Rana, T. Matsuura, Surface modifications for antifouling membranes, Chem. Rev. 110 (2010) 2448–2471.
[2] S.S. Madaeni, S. Zinadini, V. Vatanpour, A new approach to improve antifouling property of PVDF membrane using in situ polymerization of PAA functionalized TiO_2 nanoparticles, J. Membr. Sci. 380 (2011) 155–162.
[3] C. Xu, W. Huang, X. Lu, D. Yuan, S. Chen, H. Huang, Preparation of PVDF porous membranes by using PVDF-*g*-PVP powder as an additive and their antifouling property, Radiat. Phys. Chem. 81 (2012) 1763–1769.
[4] Y. Sui, Z. Wang, X. Gao, C. Gao, Antifouling PVDF ultrafiltration membranes incorporating PVDF-*g*-PHEMA additive via atom transfer radical graft polymerizations, J. Membr. Sci. 413–414 (2012) 38–47.
[5] N. Pezeshk, D. Rana, R.M. Narbaitz, T. Matsuura, Novel modified PVDF ultrafiltration flat-sheet membranes, J. Membr. Sci. 389 (2012) 280–286.
[6] A. Venault, Y. Chang, D.M. Wang, J.Y. Lai, Surface anti-biofouling control of PEGylated poly(vinylidene fluoride) membranes via vapor-induced phase separation processing, J. Membr. Sci. 423–424 (2012) 53–64.
[7] C. Zhao, X. Xu, J. Chen, F. Yang, Effect of graphene oxide concentration on the morphologies and antifouling properties of PVDF ultrafiltration membranes, J. Environ. Chem. Eng. 1 (2013) 349–354.
[8] J. Zhang, Z. Wang, X. Zhang, X. Zheng, Z. Wu, Enhanced antifouling behaviours of polyvinylidene fluoride membrane modified through blending with nano-TiO_2/polyethylene glycol mixture, Appl. Surf. Sci. 345 (2015) 418–427.
[9] G.D. Kang, Y.M. Cao, Application and modification of poly(vinylidene fluoride) (PVDF) membranes – a review, J. Membr. Sci. 463 (2014) 145–165.
[10] R. Muppalla, H.H. Rana, S. Devi, S.K. Jewrajka, Adsorption of pH-responsive amphiphilic copolymer micelles and gel on membrane surface as an approach for antifouling coating, Appl. Surf. Sci. 268 (2013) 355–367.
[11] A. Venault, Y. Chang, H.S. Yang, P.Y. Lin, Y.J. Shih, A. Higuchi, Surface self-assembled zwitterionization of poly(vinylidene fluoride) microfiltration membranes via hydrophobic-driven coating for improved blood compatibility, J. Membr. Sci. 454 (2014) 253–263.
[12] H.Y. Yu, M.X. Hu, Z.K. Xu, J.L. Wang, S.Y. Wang, Surface modification of polypropylene microporous membranes to improve their antifouling property in MBR: NH_3 plasma treatment, Sep. Purif. Technol. 45 (2005) 8–15.
[13] Q. Gu, Z. Jia, T. Zhen, Preparation of quaternized poly(vinylidene fluoride) membrane by surface photografting and its antifouling performance for alkaline proteins, Desalination 317 (2013) 175–183.
[14] Y. Li, Y. Su, X. Zhao, R. Zhang, J. Zhao, X. Fan, Z. Jiang, Surface fluorination of polyamide nanofiltration membrane for enhanced antifouling property, J. Membr. Sci. 455 (2014) 15–23.
[15] J.H. Jiang, L.P. Zhu, H.T. Zhang, B.K. Zhu, Y.Y. Xu, Improved hydrodynamic permeability and antifouling properties of poly(vinylidene fluoride) membranes using polydopamine nanoparticles as additives, J. Membr. Sci. 457 (2014) 73–81.
[16] X. Fan, Y. Su, X. Zhao, Y. Li, R. Zhang, J. Zhao, Z. Jiang, J. Zhu, Y. Ma, Y. Liu, Fabrication of polyvinyl chloride ultrafiltration membranes with stable antifouling property by exploring the pore formation and surface modification capabilities of polyvinyl formal, J. Membr. Sci. 464 (2014) 100–109.
[17] Y. Liu, Y. Su, X. Zhao, Y. Li, R. Zhang, Z. Jiang, Improved antifouling properties of polyethersulfone membrane by blending the amphiphilic surface modifier with crosslinked hydrophobic segments, J. Membr. Sci. 486 (2015) 195–206.
[18] G.R. Guillen, Y. Pan, M. Li, E.M.V. Hoeck, Preparation and characterization of membranes formed by nonsolvent induced phase separation: a review, Ind. Eng. Chem. Res. 50 (2011) 3798–3817.
[19] H. Minehara, K. Dan, Y. Ito, H. Takabatake, M. Henmi, Quantitative evaluation of fouling resistance of PVDF/PMMA-g-PEO polymer blend membranes for membrane bioreactor, J. Membr. Sci. 466 (2014) 211–219.
[20] Q. Shi, Y. Su, S. Zhu, C. Li, Y. Zhao, Z. Jiang, A facile method for synthesis of pegylated polyethersulfone and its application in fabrication of antifouling ultrafiltration membrane, J. Membr. Sci. 303 (2007) 204–212.
[21] C. Xu, W. Huang, X. Lu, D. Yan, S. Chen, H. Huang, Preparation of PVDF porous membranes by using PVDF-g-PVP powder as an additive and their antifouling property, Radiat. Phys. Chem. 81 (2012) 1763–1769.
[22] B. Liu, C. Chen, T. Li, J. Crittenden, Y. Chen, High performance ultrafiltration membrane composed of PVDF blended with its derivative copolymer PVDF-g-PEGMA, J. Membr. Sci. 445 (2013) 66–75.
[23] M. Liu, Q. Chen, L. Wang, S. Yu, C. Gao, Improving fouling resistance and chlorine stability of aromatic polyamide thin-film composite RO membrane by surface grafting of polyvinyl alcohol (PVA), Desalination 367 (2015) 11–20.
[24] J. Peng, Y. Su, Q. Shi, W. Chen, Z. Jiang, Protein fouling resistant membrane prepared by amphiphilic pegylated polyethersulfone, Bioresour. Technol. 102 (2015) 2289–2295.
[25] A. Venault, J.R. Wu, Y. Chang, P. Aimar, Fabricating hemocompatible bi-continuous PEGylated PVDF membranes via vapor-induced phase inversion, J. Membr. Sci. 470 (2014) 18–29.
[26] D.J. Lin, K. Beltsios, T.H. Young, Y.S. Jeng, L.P. Cheng, Strong effect of precursor preparation on the morphology of semicrystalline phase inversion poly(vinylidene fluoride) membranes, J. Membr. Sci. 274 (2006) 64–72.
[27] C.L. Li, D.M. Wang, A. Deratani, D. Quemener, D. Bouyer, J.Y. Lai, Insight into the preparation of poly(vinylidene fluoride) membranes by vapor-induced phase separation, J. Membr. Sci. 361 (2010) 154–166.
[28] S.T. Kao, M.Y. Teng, C.L. Li, C.Y. Kuo, C.Y. Hsieh, H.A. Tsai, D.M. Wang, K.R. Lee, J. Y. Lai, Fabricating PC/PAN composite membranes by vapor-induced phase separation, Desalination 233 (2008) 96–103.
[29] M. Gu, J. Zhang, X. Wang, H. Tao, L. Ge, Formation of poly(vinylidene fluoride) (PVDF) membranes via thermally induced phase separation, Desalination 192 (2006) 160–167.
[30] A. Mansourizadeh, A.F. Ismail, Influence of membrane morphology on characteristics of porous hydrophobic PVDF hollow fiber contactors for CO2 stripping from water, Desalination 287 (2012) 220–227.
[31] S.W. Hsiao, A. Venault, H.S. Yang, Y. Chang, Bacterial resistance of self-assembled surfaces using PPOm-b-PSBMAn zwitterionic copolymer – concomitant effects of surface topography and surface chemistry on attachement of live bacteria, Colloids Surf. B 118 (2014) 254–260.
[32] M.G. Buonomenna, P. Macchi, M. Davoli, E. Drioli, Poly(vinylidene fluoride) membranes by phase inversion: the role the casting and coagulation conditions play in their morphology, crystalline structure and properties, Eur. Polym. J. 43 (2007) 1557–1572.
[33] R. Ghosh, Z.F. Cui, Fractionation of BSA and lysozyme using ultrafiltration: effect of pH and membrane pretreatment, J. Membr. Sci. 139 (1998) 17–28.
[34] R.H. Colton, I. Pahl, L.E. Ottaviano, T. Bodeutsch, F. Meyeroltmanns, Study of protein adsorption effects on crossflow filtration using BSA and milk protein, PDA J. Pharm. Sci. Technol. 56 (2002) 20–30.
[35] M.G. Yan, L.Q. Liu, Z.Q. Tang, L. Huang, W. Li, J. Zhou, J.S. Gu, X.W. Wei, H.Y. Yu, Plasma surface modification of polypropylene microfiltration membranes and fouling by BSA dispersion, Chem. Eng. J. 145 (2006) 218–224.
[36] E.S. Hatakeyama, H. Ju, C.J. Gabriel, J.L. Lohr, J.E. Bara, R.D. Noble, B.D. Freeman, D.L. Gin, New protein-resistant coatings for water filtration membranes based on quaternary ammonium and phosphonium polymers, J. Membr. Sci. 330 (2009) 104–116.
[37] M. Hashino, K. Hirami, T. Ishigami, Y. Ohmukai, T. Maruyama, N. Kubota, H. Matsuyama, Effect of kinds of membrane materials on membrane fouling with BSA, J. Membr. Sci. 384 (2011) 157–165.

[38] C. Nie, L. Ma, Y. Xia, C. He, J. Deng, L. Wang, C. Cheng, S. Sun, C. Zhao, Novel heparin-mimicking polymer brush grafted carbon nanotube/PES composite membranes for safe and efficient blood purification, J. Membr. Sci. 475 (2015) 455–468.
[39] W.B. Tsai, J.M. Grunkemeier, T.A. Horbett, Human plasma fibrinogen adsorption and platelet adhesion to polystyrene, J. Biomed. Mater. Res. 44 (1999) 130–139.
[40] J.M. Grunkemeier, W.B. Tsai, M.R. Alexander, D.G. Castiner, T.A. Horbett, Platelet adhesion and procoagulant activity induced by contact with radio-frequency glow discharge polymers: Roles of adsorbed fibrinogen and vWF, J. Biomed. Mater. Res. 51 (2000) 669–679.
[41] N. Lebleu, C. Roques, P. Aimar, C. Causserand, Role of the cell-wall structure in the retention of bacteria by microfiltration membranes, J. Membr. Sci. 326 (2009) 178–185.
[42] C. Chong, S. Li, W. Zhao, Q. Wei, S. Nie, S. Sun, C. Zhao, The hydrodynamic permeability and surface property of polyethersulfone ultrafiltration membranes with mussel-inspired polydopamine coatings, J. Membr. Sci. 417–418 (2012) 228–236.
[43] Q. Li, Q.Y. Bi, H.H. Lin, L.X. Bian, X.L. Wang, A novel ultrafiltration (UF) membrane with controllable selectivity for protein separation, J. Membr. Sci. 427 (2013) 155–167.
[44] J. Ju, C. Wang, T. Wang, Q. Wang, Preparation and characterization of pH-sensitive and antifouling poly (vinylidene fluoride) microfiltration membranes blended with poly (methyl methacrylate-2-hydroxyethyl methacrylate-acrylic acid), J. Colloid Interface Sci. 434 (2014) 175–180.
[45] J.H. Li, M.Z. Li, J. Miao, J.B. Wang, X.S. Shao, Q.Q. Zhang, Improved surface property of PVDF membrane with amphiphilic zwitterionic copolymer as membrane additive, Appl. Surf. Sci. 258 (2012) 6398–6405.
[46] M.H. Razzaghi, A. Safekordi, M. Tavakolmoghadam, F. Rekabdar, M. Hemmati, Morphological and separation performance study of PVDF/CA blend membranes, J. Membr. Sci. 470 (2014) 547–557.
[47] M.M. Abed, S.C. Kumbharkar, A.M. Groth, K. Li, Economical production of PVDF-*g*-POEM for use as a blend in preparation of PVDF based hydrophilic hollow fibre membranes, Sep. Purif. Technol. 106 (2013) 47–55.
[48] A. Bera, C.U. Kumar, P. Parui, S.K. Jewrajka, Stimuli responsive and low fouling ultrafiltration membranes from blends of polyvinylidene fluoride and designed library of amphiphilic poly (methyl methacrylate) containing copolymers, J. Membr. Sci. 481 (2015) 137–147.